AGU100 ADVANCING EARTH AND SPACE SCIENCE

Water Resources Research

RESEARCH ARTICLE
10.1029/2017WR022353

Key Points:
- Ocean sediment temperature profiles exhibit curvature due to ocean temperature change, seabed property heterogeneity, and/or fluid flow
- New terrestrial methods for tracing groundwater from heat can account for interplay among these factors and be applied in ocean settings
- Seabed temperature profiles from the Scotian Slope suggest a submarine groundwater system with upslope recharge and downslope discharge

Supporting Information:
- Supporting Information S1

Correspondence to:
B. L. Kurylyk,
barret.kurylyk@dal.ca

Citation:
Kurylyk, B. L., Irvine, D. J., Mohammed, A. A., Bense, V. F., Briggs, M. A., Loder, J. W., & Geshelin, Y. (2018). Rethinking the use of seabed sediment temperature profiles to trace submarine groundwater flow. *Water Resources Research*, *54*. https://doi.org/10.1029/2017WR022353

Received 5 DEC 2017
Accepted 3 MAY 2018
Accepted article online 9 MAY 2018

Rethinking the Use of Seabed Sediment Temperature Profiles to Trace Submarine Groundwater Flow

B. L. Kurylyk[1], D. J. Irvine[2], A. A. Mohammed[3], V. F. Bense[4], M. A. Briggs[5], J. W. Loder[6], and Y. Geshelin[6]

[1]Department of Civil and Resource Engineering and Centre for Water Resources Studies, Dalhousie University, Halifax, Nova Scotia, Canada, [2]College of Science and Engineering and National Centre for Groundwater Research and Training, Flinders University, Adelaide, South Australia, Australia, [3]Department of Geoscience, University of Calgary, Calgary, Alberta, Canada, [4]Department of Environmental Sciences, Wageningen University, Wageningen, The Netherlands, [5]Hydrogeophysics Branch, U.S. Geological Survey, Hydrogeophysics Branch, Storrs, CT, USA, [6]Fisheries and Oceans Canada, Bedford Institute of Oceanography, Dartmouth, Nova Scotia, Canada

Abstract Submarine groundwater fluxes across the seafloor facilitate important hydrological and biogeochemical exchanges between oceans and seabed sediment, yet few studies have investigated spatially distributed groundwater fluxes in deep-ocean environments such as continental slopes. Heat has been previously applied as a submarine groundwater tracer using an analytical solution to a heat flow equation assuming steady state conditions and homogeneous thermal conductivity. These assumptions are often violated in shallow seabeds due to ocean bottom temperature changes or sediment property variations. Here heat tracing analysis techniques recently developed for terrestrial settings are applied in concert to examine the influences of groundwater flow, ocean temperature changes, and seabed thermal conductivity variations on deep-ocean sediment temperature profiles. Temperature observations from the sediment and bottom ocean water on the Scotian Slope off eastern Canada are used to demonstrate how simple thermal methods for tracing groundwater can be employed if more comprehensive techniques indicate that the simplifying assumptions are valid. The spatial distribution of the inferred groundwater fluxes on the slope suggests a downward groundwater flow system with recharge occurring over the upper-middle slope and discharge on the lower slope. We speculate that the downward groundwater flow inferred on the Scotian Slope is due to density-driven processes arising from underlying salt domes, in contrast with upward slope systems driven by geothermal convection. Improvements in the design of future submarine hydrogeological studies are proposed for thermal data collection and groundwater flow analysis, including new equations that quantify the minimum detectable flux magnitude for a given sensor accuracy and profile length.

1. Introduction

Submarine groundwater discharge (SGD) facilitates mass, solute, and potentially thermal exchanges between the ocean and adjacent or underlying aquifers (Beusen et al., 2013; Johannes, 1980; Li et al., 1999; Slomp & Van Cappellen, 2004; Wilson et al., 2015). Depending on the ocean depth, these exchanges can be driven by many processes (Santos et al., 2012), including tidal cycles (Heiss & Michael, 2014; Robinson et al., 2007), seasonal aquifer variations (Michael et al., 2005), and sea level rise (Werner et al., 2013). SGD includes fresh and saline components, with the former sourced by terrestrial recharge and the latter sourced by marine recharge recirculated across the sediment-ocean interface (Burnett et al., 2003; Sawyer et al., 2016; Wilson, 2005). Recirculated saline SGD impacts a number of processes such as solute oxidation, heat flow, sediment diagenesis, and microbially mediated mineralization of organic matter; thus, shallow interactions between submarine aquifers and seawater are an important aspect of marine biogeochemical cycles and thermal dynamics (Kuhn et al., 2017; Wilson, 2003; Zektser & Dzhamalov, 2007). The number of studies investigating SGD has rapidly increased in recent years across many research disciplines (Moore, 2010), but there is a widely recognized need for such investigations to be better grounded in hydrogeological knowledge (Kazemi, 2008; Post et al., 2013). Also, as reviewed by Sawyer et al. (2016) and Michael et al. (2017), most recent submarine groundwater research has focused on relatively shallow, coastal regions given their obvious societal relevance. Fewer studies have investigated the existence and/or driving processes of submarine groundwater systems in deeper marine environments, though their spatial extent and gross fluxes likely dwarf those of shallow continental margins.

A range of physical and geochemical methods have been developed and applied to trace SGD (e.g., Burnett et al., 2006; Taniguchi et al., 2002), with each characterized by its own assumptions, uncertainties, and limitations. Heat is a natural groundwater tracer that is used to qualitatively or quantitatively study groundwater flow by capitalizing on the understanding that groundwater movement induces heat advection and influences subsurface thermal regimes (Anderson, 2005; Saar, 2011). Standard approaches rely on either steady state techniques, which infer groundwater fluxes from presumably static subsurface temperature-depth profiles (Bredehoeft & Papadopulos, 1965; Kurylyk et al., 2017; Shan & Bodvarsson, 2004), or transient techniques that estimate fluxes from the downward propagation of diel to decadal surface temperature changes (Goto et al., 2005; Hatch et al., 2006; Kurylyk & Irvine, 2016; Luce et al., 2013; Stallman, 1965; Taniguchi et al., 1999). A few studies have used transient thermal signals to trace groundwater in marine or coastal settings where tides, waves, and other hydrodynamic processes, coupled with variations in the surface energy budget, can create time-varying ocean temperature signals that penetrate into the shallow sediment (e.g., Befus et al., 2013; Goto et al., 2005; Wilson et al., 2016).

Seabed temperature data in deep marine settings (e.g., $>$1,000 m of ocean depth) are available in many locations around the globe as ocean scientists have long been interested in obtaining measurements of seabed heat flow (Bullard, 1954) and relating these measurements to global energy budgets, ocean lithosphere age, plate tectonics, and marine hydrogeology (Davis & Elderfield, 2004; Wright & Louden, 1989). Ocean sediment temperature-depth profiles are usually recorded from a ship by lowering a gravity-driven probe containing a string of thermistors down into seabed depths of 5 to 10 m (Davis et al., 1984; Louden & Wright, 1989). As more seabed temperature data became available, many scientists noted that the thermal profiles often exhibited curvature, which they attributed to vertical fluid flow (Abbott et al., 1981; Anderson et al., 1979; Fisher & Becker, 1991; Geller et al., 1983; Wheat et al., 2004). Groundwater fluxes in these studies were usually quantified from the curvature of temperature-depth profiles via the classic Bredehoeft and Papadopulos (1965) method, which is an analytical solution to a heat flow equation that assumes steady state and homogeneous conditions. The steady state assumption was invoked based on the high thermal inertia of the ocean and presumed limited temperature variability in deep marine settings. Deep temperature profiles have also been recorded in oceanic crust boreholes and analyzed to infer fluid fluxes and/or permeability (e.g., Harris & Higgins, 2008).

Several studies later questioned the validity of using the temperature profile curvature in seabed sediment to estimate groundwater fluxes given that, even in deep environments, profile curvature can arise due to other factors besides heat advection, including temporal change in bottom water temperature (BWT, i.e., temperature in the ocean's "bottom mixed layer"; e.g., Armi & Millard, 1976) and vertical variation in sediment thermal conductivity (Fisher, 2004; Langseth & Herman, 1981; Louden & Wright, 1989; Noel, 1984). Both increasing BWT and decreasing thermal conductivity with depth cause concave-upward temperature profiles, similar to the effects of downward groundwater flow. Conversely, both decreasing BWT and increasing thermal conductivity with depth create convex-upward profiles, similar to the impacts of upward groundwater flow. Similar observations have also been made for terrestrial temperature profiles (Reiter, 2005). Previous studies that examined sources of ocean sediment temperature profile curvature have considered either heat advection *or* other factors such as BWT change and heterogeneity. The present study employs recently developed analysis techniques to unravel the relative importance of multiple concurrent sources of thermal perturbations in seabed sediments. As we detail in this study, using heat to investigate deep-ocean submarine hydrogeological processes is challenging and characterized by uncertainty, but other submarine hydrogeological investigation techniques are often prohibitively expensive and involve technical and logistical challenges.

The overall goals of this study are to investigate the challenges associated with using heat to trace submarine groundwater flow in deep marine environments and to determine the ability of heat tracing methods recently developed for terrestrial settings to overcome such challenges. Near-bottom ocean and sediment temperature data collected on the continental slope off the Atlantic coast of Canada (Negulic & Louden, 2017) are analyzed to map spatial patterns of submarine groundwater flow. The specific study objectives are to (1) examine how BWT fluctuations or thermal conductivity variations can induce curvature in seabed thermal profiles and create the appearance of groundwater flow, (2) investigate the downward propagation of BWT changes to determine the depths at which thermal profiles can justifiably be analyzed with steady state methods to estimate groundwater fluxes, (3) analyze the spatial distribution of inferred groundwater fluxes to provide insight into the continental slope submarine groundwater flow system in the study region, and (4) provide guidance for future studies.

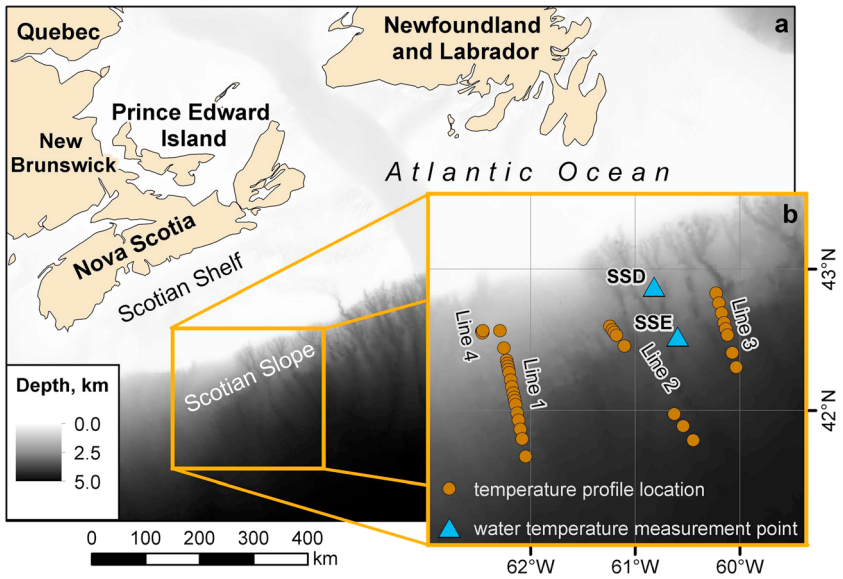

Figure 1. (a) Map of study site location with respect to Nova Scotia, Canada, and (b) locations (inset) of thermal profiles (orange) and near-bottom ocean temperature time series (blue triangles) at the Scotian Slope study site overlaid on top of bathymetry data from Shaw and Courtney (2004).

2. Study Site and Data Collection

2.1. Site Location and Geology

The Scotian Slope and Rise (Figure 1a) extend southeastward from the Scotian Shelf (typical water depths of 100–300 m) off the Canadian province of Nova Scotia to the Sohm Abyssal Plain (depths exceeding 4,500 m). The study region spans portions of the slope and rise, with water depths in the 1,500–4,500-m range; but for simplicity, we refer to both the slope and rise hereafter as the Scotian Slope (Figure 1b). The geology of the area is composed of a thick deposit (up to 16 km in the deep subbasins) of marine sediments underlain by a continental crust that thins away from the continent due to plate rifting (Jansa & Wade, 1975; Negulic, 2010; Negulic & Louden, 2017). Coarse surficial geological mapping of the slope revealed large deposits of sand and gravel at the crest and more mud and other finer-grained material toward the toe (Piper & Campbell, 2002). Also, a cursory analysis of grain size distribution data taken from 42 samples in the study region and provided by the Geological Survey of Canada (2017; Supporting Information Figure S1) revealed that the slope sediment was on average 2% gravel, 12% sand, 31% silt, and 55% clay. Thus, although no direct hydraulic conductivity (K) tests were conducted, we expect the order of magnitude of K averaged across the study region to be in the low end of the K range for sandy silts or high end for clays (e.g., 10^{-8} to 10^{-7} m/s; Fetter, 2001, p. 84). However, some samples contained much higher percentages (maximum 65%) of sand and gravel, and thus, K likely has considerable spatial variability with the potential for higher-K preferential flow paths.

Large buried salt domes in the study region were delineated using geophysical techniques (Negulic & Louden, 2017). These have been known to influence the regional heat flow distribution and submarine groundwater flow system in other study regions due to the physical structure of the domes, the resulting hydraulic and thermal conductivity distribution, and the influence of salinity on water density (e.g., Wilson & Ruppel, 2007).

2.2. Thermal Data Collection on the Scotian Slope

The seabed thermal data considered in this study were collected in 2004 (Line 4, Figure 1b) and 2008 (Lines 1–3) and have been previously reported and analyzed to map the Scotian Slope heat flow distribution (Negulic & Louden, 2017). The thermal surveys were conducted from the vessel CCGS Hudson using the Dalhousie Heat Flow and Thermal Conductivity Probe described in detail by Louden et al. (1997). The probe extends to depths of almost 6 m and contains a string of 32 evenly spaced (18-cm separation) thermistors with a precision and accuracy of 0.001 °C and a resolution of 0.00001 °C (Negulic, 2010).The thermistors were calibrated by first recording a thermal profile in the thermally uniform ocean water column immediately above the bed to standardize the thermistor readings (Negulic, 2010). This probe design also allows for the thermal properties of

the surrounding sediment to be obtained from the radial decay of an engineered heat pulse. The series of equations required for this step has been described in several papers (e.g., Lister, 1979). In total, 47 temperature profiles were measured, but only 40 (Figure 1b) were analyzed in the present study due to issues arising from profiles without a corresponding heat pulse measurement, with a high number of missing data points, or with extreme scatter in the temperature data. Due to the calibration procedure, the sediment thermal probe only measures sediment temperature relative to the bottom water temperature (BWT; Negulic, 2010).

In addition to the sediment temperature and derived thermal conductivity data collected by Negulic and Louden (2017), time series of near-bottom ocean temperature from sites SSD (2,400-m depth) and SSE (3,400-m depth; Figure 1b) were available for the period 7 October 2007 to 1 October 2008 from a Bedford Institute of Oceanography moored measurement program. The program used Seabird Scientific SBE37 MicroCAT temperature-salinity recorders moored at 10 m above the seabed, sampling at 5-min intervals. Direct observations of vertical temperature profiles in the bottom 10 m of the ocean column in the study region (results not shown) indicate that vertical temperature gradients there are effectively negligible, as in other deep-ocean bottom boundary layer studies (Armi & Millard, 1976). Thus, in this study, these ocean water temperature records were assumed to be representative of the BWT.

In general, the thermal data available to this study are more useful in comparison to those available for many of the early studies using heat to trace deep-ocean SGD because the temperature values were collected at a relatively high vertical resolution (0.18 m) and included the heat pulse analysis to also yield an estimated thermal conductivity. Furthermore, most previous studies of this nature did not have access to multimonth records of BWT variations, which can provide insight into how temperature profile curvature may be caused by transience (i.e., deviation from a steady state regime) rather than by groundwater flow.

3. Methods: Thermal Analysis

3.1. Potential Additional Sources of Profile Curvature

The three potential sources of temperature profile curvature considered in detail below are vertical groundwater flow, BWT variations, and thermal conductivity variation. Noel (1984) lists several additional factors that can induce profile curvature: sampling disturbance, frictional heating, variable bottom currents, sediment heat production or absorption, topographic effects, and sedimentation effects. Frictional heat effects for the study site data are accounted for in the profile analysis (Negulic, 2010). The curvatures in the measured temperature profiles in this study are both concave upward and convex upward as described later. Since sampling disturbance, heat production/absorption, and sediment effects create regionally coherent curvatures (Noel, 1984), it is unlikely that any of these processes are the dominant causes of the highly variable curvatures observed at the study site. Topographic effects due to the slope were considered with a two-dimensional, steady state conductive heat flow simulation in the numerical heat transfer model FlexPDE (e.g., Bense & Kooi, 2004). The numerical modeling results (see supporting information Figure S2) indicate that the geometry of the Scotian Slope does not induce temperature profile curvature in the upper 6 m. In general, detailed analyses by previous studies (Langseth & Herman, 1981; Noel, 1984) have shown that while all of these factors are possible, the most common sources of profile curvature are the three considered in this study.

3.2. Overview of Thermal Methods and Description of Transient Method

It is important to note that the sediment temperature profiles were only available at a single instant in time. Transient techniques to trace groundwater using heat are more powerful than steady state methods, but the former are difficult to validate without some knowledge of the temperature profile change over time (Bense et al., 2017; Bense & Kurylyk, 2017). Furthermore, the measured profiles are spread across a spatially extensive region with only two BWT records from the period immediately prior to the available seabed thermal profiles (Figure 1b). Because BWT on the Scotian Slope has some spatial structure, data from the two sensors could not be used to directly form transient thermal boundary conditions for all profiles within the entire study region. Thus, transient approaches to directly estimate groundwater fluxes are not feasible for this study.

To overcome these limitations, we first applied a transient method to determine a depth below which the thermal regime can be considered to be at steady state based on the magnitude of typical BWT variations. Next, we applied simpler, steady state methods to this lower zone to estimate the groundwater fluxes for each profile. By adopting this approach, we circumvent the need for time series of BWT at each station or repeated profiles of sediment temperature. An overview of the methods used in this study is presented in

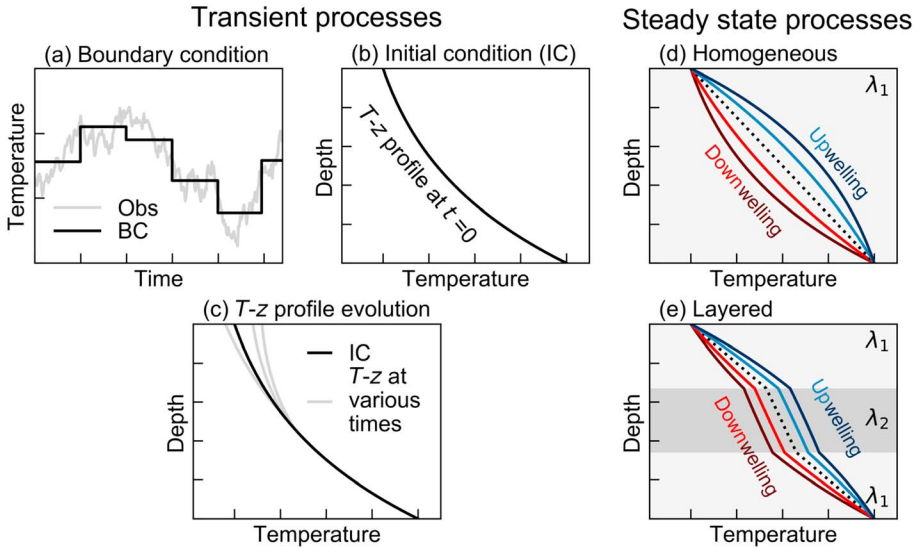

Figure 2. (a–c) The transient method (FAST model) used in the study (Kurylyk & Irvine, 2016). (a) The boundary conditions based on the measured BWT data (b) disturb the initial conditions, (c) creating transience in the shallow zone of the temperature profiles but retaining steady state conditions in the lower portion of the profiles. (d, e) Steady state methods used in this study. The simplest equation (Bredehoeft & Papadopulos, 1965; equation (5)) can be used to estimate flux from temperature profile curvature (d), but thermal conductivity variation can also create curvature at steady state (e; Shan & Bodvarsson, 2004). In (e) λ_2 is the thermal conductivity of the second layer and is greater than λ_1.

Figures 2 and 3 and described in detail below. Given the order of the data analysis workflow, the transient method is detailed first.

Vertical subsurficial heat transfer is often represented by the one-dimensional (vertical), transient conduction-advection equation (Stallman, 1963):

$$\lambda \frac{\partial^2 T}{\partial z^2} - q c_w \rho_w \frac{\partial T}{\partial z} = c\rho \frac{\partial T}{\partial t} \tag{1}$$

where λ is the bulk thermal conductivity of the medium ($W \cdot m^{-1} \cdot °C^{-1}$), T is temperature (°C), z is depth from surface (m), q is the vertical Darcy flux (m/s, positive downwards), t is time (s), c_w and c are respectively the specific heats of the water and the saturated medium ($J \cdot kg^{-1} \cdot °C^{-1}$), and ρ_w and ρ are the water and saturated medium densities (kg/m^3). The right-hand side represents the heat storage change term, and the first and second terms on the left-hand side, respectively, represent the negative divergences of the conductive and advective heat fluxes. The methods described in this study only yield the vertical Darcy flux (q); thus, for simplicity we hereafter use the term "flux" to refer specifically to the vertical component of the Darcy flux.

Equation (1) is the governing equation from which analytical solutions have been obtained for a periodic boundary condition to represent diel or seasonal surface water temperature variability (e.g., Luce et al., 2013; Stallman, 1965). Such approaches have been commonly applied to trace stream-aquifer exchanges across a streambed interface (e.g., Hatch et al., 2006; Rau et al., 2014). The standard analytical solution (Stallman, 1965) to equation (1) subject to a periodic boundary condition can be rearranged to isolate for the decay depth of a periodic signal (Briggs et al., 2014):

$$Z_d = \frac{2\lambda}{c\rho}\left[\frac{\ln\left(A_{min}/A_0\right)}{v_t - \sqrt{\left\{v_t^4\left[1+\left(\frac{8\pi\lambda}{c\rho P v_t^2}\right)^2\right]\right\}^{1/2} + \frac{v_t^2}{2}}}\right] \tag{2}$$

where Z_d is the decay depth (m) of the periodic signal below which the thermal regime is steady, A_0 is the amplitude of the periodic signal at the surface (°C), A_{min} is the minimum detectable amplitude (°C), v_t is the thermal front velocity due to advection ($v_t = qc_w\rho_w/(c\rho)$, m/s), and P is the period of the signal (s). Here A_{min} is taken following Briggs et al. (2014), as twice the sensor precision (0.002 °C). In theory, equation (2)

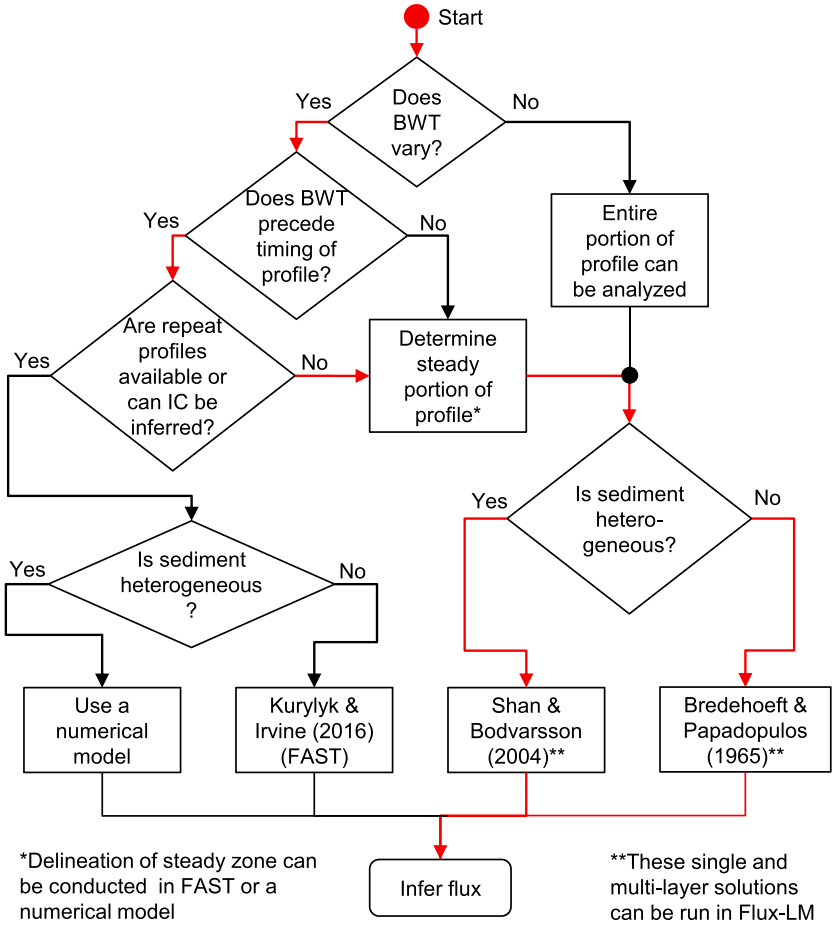

Figure 3. Approaches for using sediment temperature profiles collected in deep-ocean environments to trace groundwater flow. The recommended approach is influenced by potential complications due to transient effects or heterogeneities. Red arrows indicate the paths that were taken in the present study.

can be used to separate the steady state and transient zones assuming repeating periodic signals. As will be shown, this approach was overly conservative compared to the FAST method described below, so the FAST results were ultimately applied to delineate the steady state zone.

For heat transfer in deep-ocean sediment, the surface boundary condition is formed from the BWT variations, which are not typically periodic. Thus, a nonperiodic boundary condition form may be preferred. A multistep boundary condition (Figure 2a) is sufficiently flexible to represent any complex or intermittent temperature changes that are neither periodic nor continuously increasing (Menberg et al., 2014):

$$\text{Boundary condition}: \quad T(z=0,t) = T_0 + \sum_{j=1}^{n} \Delta T_j \times H\left(t - t_j\right) \tag{3}$$

where T_0 is the initial surface temperature (°C), ΔT_j is the jth surface temperature shift (°C) evaluated as the thermal difference before and after shift j, t_j represents the timing of shift j (s), and H is the Heaviside function that turns the steps on at the appropriate times (i.e., $H\,(t - t_j) = 0$ before t_j and 1 after t_j).

Transient methods with non-periodic signals also require an initial condition, and the most flexible form is a nonlinear function (Figure 2b), which can be used to match steady state or transient temperature profiles influenced by advection (Kurylyk & MacQuarrie, 2014):

$$\text{Initial condition}: \quad T(z, t=0) = T_i + az + \delta \exp(dz) \tag{4}$$

where $T_i + \delta$ is equivalent to the initial surface temperature (T_0, °C), a is the geothermal gradient (°C/m), and d (m^{-1}) is a fitting parameter to account for curvature in the temperature profile due to vertical groundwater flow or past surface temperature change.

Kurylyk and Irvine (2016) derived an analytical solution to equation (1) for a semi-infinite domain subject to the boundary condition in equation (3) and the initial condition in equation (4). The resultant solution, which is not reproduced here due to its length, employs superposition principles and allows for any number of step changes in the surface temperature. The solution is coded into the Python model FAST (Flexible Analytical Solution using Temperature; Kurylyk & Irvine, 2016). FAST enables the user to convert a measured surface temperature time series into a multistep boundary condition (e.g., Figure 2a), perform the solution calculations (i.e., forward model from the initial condition), and infer the optimal groundwater flux by adjusting the flux to minimize the differences between calculated and measured temperature profiles. FAST has been applied to estimate fluxes from terrestrial borehole profiles in Japan (Kurylyk & Irvine, 2016), Australia (Irvine et al., 2017), and the Netherlands (Bense et al., 2017). In this study, FAST is applied to delineate transient and steady state zones (Figure 2c) for typical Darcy flux magnitudes using measured BWT variations, sediment temperature, and thermal conductivity.

3.3. General Description of Steady State Methods

Two steady state methods were employed in this study. The first (Bredehoeft & Papadopulos, 1965) assumes homogeneous conditions, while the second (Shan & Bodvarsson, 2004) accounts for potential variations in the medium thermal conductivity with depth. The influence of seabed thermal conductivity was considered as it is one postulated source of seabed thermal profile curvature (Noel, 1984). Bredehoeft and Papadopulos (1965) derived a solution (Figure 2b) to a steady state form of equation (1) for a finite, homogeneous domain with fixed temperatures at the surface (T_0, °C) and bottom (T_L, °C) located at depth L (m):

$$T(z) = T_0 + (T_L - T_0)\frac{\exp(\beta z/L) - 1}{\exp(\beta) - 1} \tag{5}$$

where β is the dimensionless Peclet number for the domain considered ($c_w\rho_w qL/\lambda$). This equation was originally developed with the top and lower boundaries imposed at upper and lower confining units, respectively; however, the equation has been applied successfully in diverse field and numerical environments, including streambeds (Caissie et al., 2014) and deep aquifers (Irvine et al., 2016), using any points within a homogeneous medium to form the boundary locations. It should be noted that an alternative solution can be easily derived that is equivalent to the Bredehoeft and Papadopulos (1965) conceptual model and solution, except that a constant heat flux, rather than temperature, is assigned at the lower boundary (Harris & Chapman, 1995). We chose to use the approach with a specified lower temperature (equation (5)), as this temperature is measured directly by the lowest thermistor and, unlike heat flux, it does not rely on a thermal gradient estimated from the temperatures and elevations of the two lowest thermistor readings.

Shan and Bodvarsson (2004) derived a steady state, conduction-advection solution like equation (5), but for multilayered systems with each layer characterized by different thermal conductivities (Figure 2e). This thermal conductivity variation can induce profile curvature even in the absence of groundwater flow. The spreadsheet tool Flux-LM (Flux in Layered Media) was developed to quickly run either the Bredehoeft and Papadopulos (1965) solution or the Shan and Bodvarsson (2004) solution to infer groundwater fluxes from the shape of temperature profiles in homogeneous or layered media (Kurylyk et al., 2017). In this study, root-mean-square error (RMSE) values were calculated between the measured temperature profiles and the optimal analytical solution fits, and fits yielding RMSE values <0.005 °C were considered good.

3.4. Specific Thermal Analysis Workflow for the Present Study

A general workflow for analyzing seabed temperature-depth profiles for submarine groundwater flow is presented in Figure 3, with the workflow of the present study indicated by the red arrows.

As previously noted, the FAST model was applied in addition to equation (2) to determine the penetration depth of BWT signals and the approximate steady state zones at the study site. Steady state FAST initial conditions were generated for both downwelling and upwelling scenarios to assess the role of the groundwater flow direction on BWT signal propagation. Steady state initial conditions were chosen based on the assigned Darcy flux and the average of the BWT series. This prevented the deeper portions of the profile from thermally changing during the forward modeling due to the system adjusting from out-of-sync initial conditions. The initial conditions for the downwelling FAST run were based on a measured sediment temperature profile on the Scotian Slope (Station 117r, Negulic & Louden, 2017) that was representative of average conditions

across the study site in terms of both the measured bulk thermal conductivity (1.079 W · m · °C) and the thermal gradient (0.045 °C/m). As the thermal probe recorded temperatures relative to the BWT, the absolute temperatures for this profile were obtained by setting the top surface temperature of the sediment profile equal to the average BWT and shifting all temperature values accordingly. The steady state Bredehoeft and Papadopulos (1965) solution (equation (5)) was used to generate a temperature profile fitted to this measured profile, and a downwelling flux of q = 0.94 m/yr was inferred based on the solution fit across the entire profile (RMSE = 0.01 °C). This flux magnitude was representative of magnitudes estimated across the Scotian Slope as discussed later (section 4.3). Steady state initial conditions for an *upwelling* FAST scenario were obtained by changing the direction of the Darcy flux (i.e., $q = -0.94$ m/yr) in the Bredehoeft and Papadopulos (1965) equation but otherwise using the same parameters as above for the downwelling scenario (i.e., the same boundary temperatures and thermal properties based on Station 117 were used to consider a hypothetical, steady state upwelling scenario).

The final step in the generation of the FAST initial conditions was to apply equation (4) to achieve fits to the upwelling and downwelling steady state profiles generated with equation (5). This additional step is required as equation (5) is for a finite domain but FAST is for a semi-infinite domain. Fits between equations (4) and (5) yielded RMSE values $\leq$0.0004 °C. Figure S3 and Table S1 in the SI show the measured profile (Station 117r), and the solution fits and parameters from equations (4) and (5) used to generate the initial conditions for the FAST upwelling and downwelling runs.

The measured near-bottom ocean temperatures (SSD and SSE sites, Figure 1b) were used to generate a multistep boundary condition (equation (3)) by averaging the measured temperature time series for 5-day intervals for the data record available from October 2007 to October 2008. FAST was employed to forward model the initial conditions described above using the boundary condition (e.g., Figure 2a). The forward modeling was conducted for approximately 1 year (8 October 2007 to 1 October 2008) based on the BWT deployment time period, and a consistent Darcy flux was used in the initial conditions and forward modeling for both the upwelling and downwelling scenarios. The temperature profiles outputted by FAST throughout this period were investigated to assess the penetration depth of the BWT signals and to delineate transient and steady state zones (Figure 2c). The relative error (E, %) in the Darcy flux inferred from the FAST-outputted temperature profiles using the steady state method (q_{steady}, m/yr) compared to the actual Darcy flux employed in the FAST modeling (q_{act}, m/yr) was calculated at each output time with equation (6).

$$E = \frac{q_{\text{steady}} - q_{\text{act}}}{abs|q_{\text{act}}|} \times 100\% \tag{6}$$

Finally, after delineating the steady state zone based on the FAST results, the steady state portions of the measured profiles from the Scotian Slope were analyzed to infer submarine groundwater recharge and discharge fluxes using homogeneous and multilayer steady state methods (Figures 2d and 2e).

4. Results and Discussion

4.1. Transient Analyses in FAST

Figure 4a presents the BWT data recorded at the mooring sites SSD and SSE indicated in Figure 1b. The BWT data were analyzed with the standard Signal Processing Toolbox in Matlab (The MathWorks, Inc., 2014), which indicated a maximum amplitude and period for this time series of 0.15 °C and 25 days, respectively. These BWT variations on the Scotian Slope are expected to arise primarily from some combination of variability in the North Atlantic's Deep Western Boundary Current carrying subpolar waters equatorward and topographic Rossby waves generated by energetic Gulf Stream meanders and rings (e.g., Peña-Molino et al., 2012; Smith et al., 2016; Toole et al., 2017). The amplitudes of the observed BWT variations are comparable in magnitude to those observed at other sites with similar ocean depths (Davis et al., 2003). Both the amplitude and the period of the BWT variations are important in terms of the signal penetration depth (equation (2)). Although the SSD and SSE temperature time series are different due to their different positions (especially water depths), the periods and amplitudes of BWT fluctuations are similar. An analysis of BWT time series recorded in subsequent years and multiple locations across the study site (results not shown) further revealed that the BWT fluctuation amplitudes across the Scotian Slope are similar from site to site. Thus, to

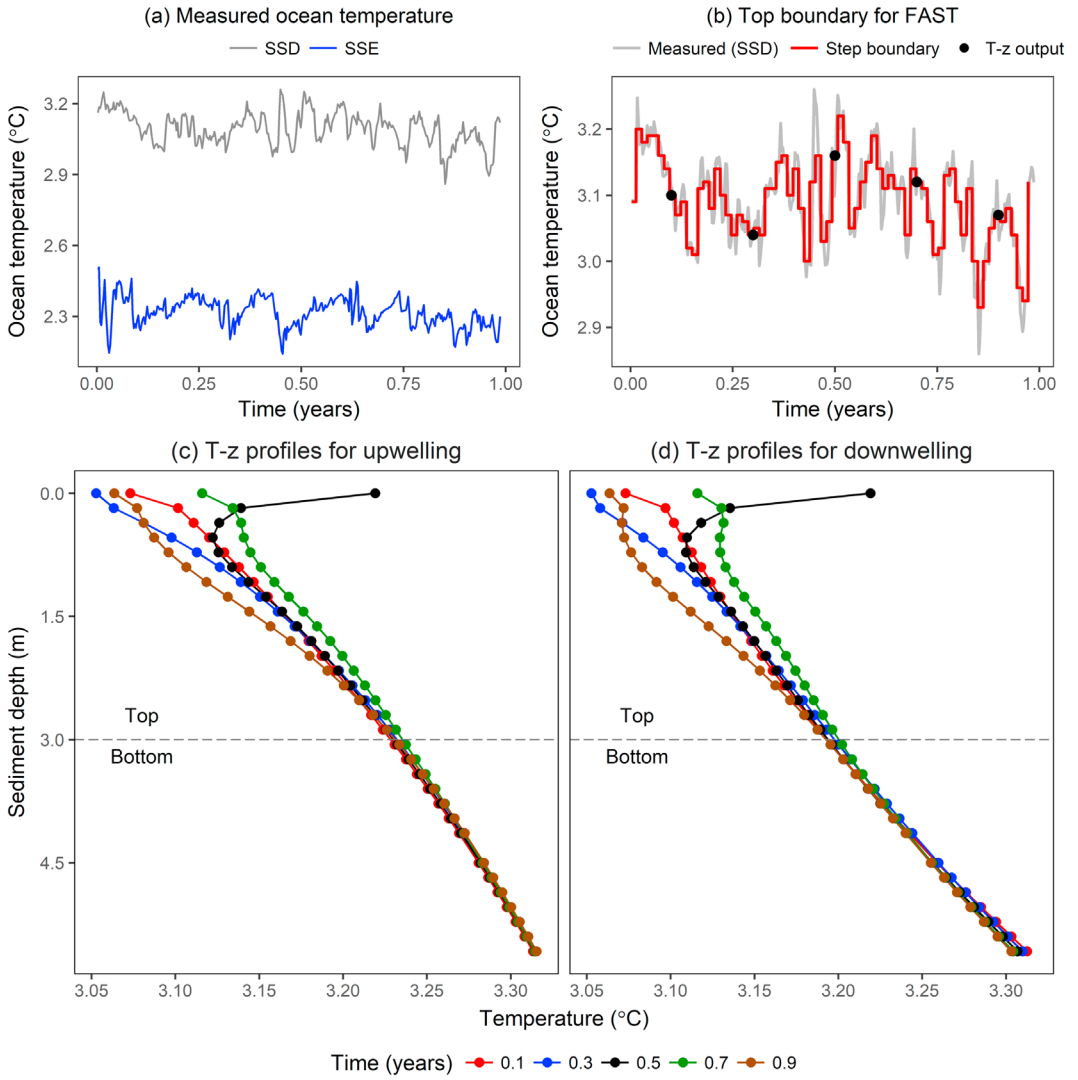

Figure 4. (a) Mean daily deep-ocean water temperature time series at the SSD and SSE sites. (b) Boundary condition (red) fit to the measured SSD data with step lengths of 5 days. The output times for the FAST model results shown in (c) and (d) are indicated by the black circles. (c and d) Intra-annual, temperature-depth (*T-z*) profiles generated in FAST using the initial condition described in the text perturbed by the boundary condition shown in (b) for upwelling (c) and downwelling (d). The vertical flux magnitude was 0.94 m/yr (section 3.4). Time = 0 occurs at 8 October 2007.

examine the influence of BWT at a representative site, only the SSD site (Figures 1b and 4a) was used to create the FAST multistep boundary condition (red series, Figure 4b). The SSD site was chosen because it had a slightly higher range (0.48 °C) between the maximum and minimum BWT compared to the SSE site (0.41 °C).

The FAST modeling was conducted for approximately 1 year (Figure 4) and thus did not consider very low frequency (multidecadal) trends in BWT such as have been measured or postulated in previous studies (Fukasawa et al., 2004; Harris & the IODP Expedition 306 Scientists, 2006; Johnson et al., 2007). However, the seabed temperature profile curvature induced by decadal warming should be in the same direction across the study site, unlike what was observed on the Scotian Slope (section 4.3). Also, although decadal BWT signals would be expected to shift the temperature profiles to the right (increasing temperature) on a multidecadal timescale, transient 1-D conduction modeling in FlexPDE (results not shown) indicates that persistent, multidecadal BWT warming rates observed in deep-ocean settings (e.g., up to 0.01 °C/yr) could not induce the degree of curvature described later for temperature profiles less than 10-m deep. Decadal warming is too slow to cause this curvature because new quasi-equilibrium conditions are achieved.

Figures 4c and 4d respectively show the temperature profiles outputted by FAST for upwelling and downwelling conditions at times of 0.1, 0.3, 0.5, 0.7, and 0.9 years, with 8 October 2007 treated as $t = 0$. Since the amplitudes of the BWT variations were relatively consistent across the site as described above, these results should represent typical intra-annual sediment temperature profile variations at the study site based on the boundary condition formed with measured BWT variations and the representative initial conditions (Table S1). The temperature profiles produced by FAST (see symbols, Figures 4c and 4d) are at a coarse spatial resolution to match the spatial resolution (0.18 m) of the measured temperature profiles. Table S3 of the supporting information contains the numerical values for these profiles.

Figures 4c and 4d clearly indicate that the amplitudes of the intra-annual temperature variation decrease substantially with depth. The bottom boundary in the FAST model is at a depth of infinity, and thus, the thermal constancy at depth is not a boundary condition artifact. The temperature profiles did not exhibit much intra-annual variation below depths of about 3 m as indicated by the fact that the data points below this depth for each output time essentially overlie each other regardless of the flux direction (Figures 4c and 4d). The very minor differences ($<$0.01 °C) in the bottom part of the downwelling profiles (Figure 4d) reflect offsets in the temperature profiles introduced by the imperfect matching of equations (4) and (5) to generate initial conditions. FAST was also run with a constant surface boundary condition, and the minor variations at depth were still present and consequently cannot be attributed to BWT variations. The BWT signal penetration depths modeled in FAST can be compared to that calculated with the simple periodic decay approach (equation (2) and Figure 5a). For the amplitude and period noted above, the decay depth produced by equation (2) is 1.55 m (white symbol, Figure 5a) using other representative conditions for the study site. Since FAST employs a more flexible boundary condition (equation (3)) for the stochastic and relatively nonperiodic boundary time series (Figure 4a), the greater penetration depth modeled by FAST (~3 m, Figures 4c and 4d) is more realistic than that found from the periodic signal decay method.

In general, when applying steady state techniques, there is a trade-off between maximizing the length of the zone being analyzed (see section 5.2) and lowering the top boundary to remove or minimize any BWT signal effects. The steady state Bredehoeft and Papadopulos (1965) solution was applied to study the FAST-generated temperature profiles for scenarios with the top boundary shifted down to depths of 2, 3, and 4 m. This analysis revealed that the zone between 2 and 3 m was too transient (range of 0.020 °C) to apply steady state techniques, while the zone below 4 m did not contain enough data points or length to accurately characterize the profile curvature. The profile portion below 3 m was sufficiently long to apply the Bredehoeft and Papadopulos (1965) solution (see section 5.2), but there were some minor temporal variations (range of 0.0067 °C) at 3 m. The zone above 3 m is herein denoted as the "top zone," while depths below 3 m are referred to as the "bottom zone" (Figures 4c and 4d). The following section determines if the minor temperature variations below 3 m are sufficient to influence the steady state analyses and impact the magnitude or direction of inferred Darcy flux.

4.2. Steady State Analysis of the FAST-Modeled Profiles

To examine the potential influence of BWT variations on the temperature profile curvature above and below 3 m, the FAST-outputted profiles (Figure 4) were analyzed with the Bredehoeft and Papadopulos (1965) solution in Flux-LM for the top and bottom zones to infer the Darcy fluxes under presumed steady state conditions. Due to its highly transient nature, the top surface temperature value for all FAST-outputted profiles was excluded from these steady state analyses. Since the actual vertical Darcy fluxes ($q = \pm 0.94$ m/yr for upwelling and downwelling) used in the FAST modeling are known, the accuracy of the steady state approach in the context of variable BWT can be evaluated directly using the relative error in the inferred flux (E, equation (6)). In general, the fluxes estimated from the top and bottom zones varied substantially in magnitude and direction.

On average, the bottom zone E magnitude for all output times and for groundwater flow in both directions was only 22%, but the average top zone E for the same scenarios was much larger at 310%. Clearly, the top zone yields E values that are unreasonably high; however, the bottom zone yields an acceptable average E given the considerable uncertainty of every submarine groundwater tracing method (e.g., Burnett et al., 2006; Taniguchi et al., 2002). In addition to E, we also considered the RMSE (°C) between the FAST-outputted profiles and the temperature profiles generated by the Bredehoeft and Papadopulos (1965) solution, with RMSE values less than 0.005 °C considered good fits. The E value quantifies the error associated with the

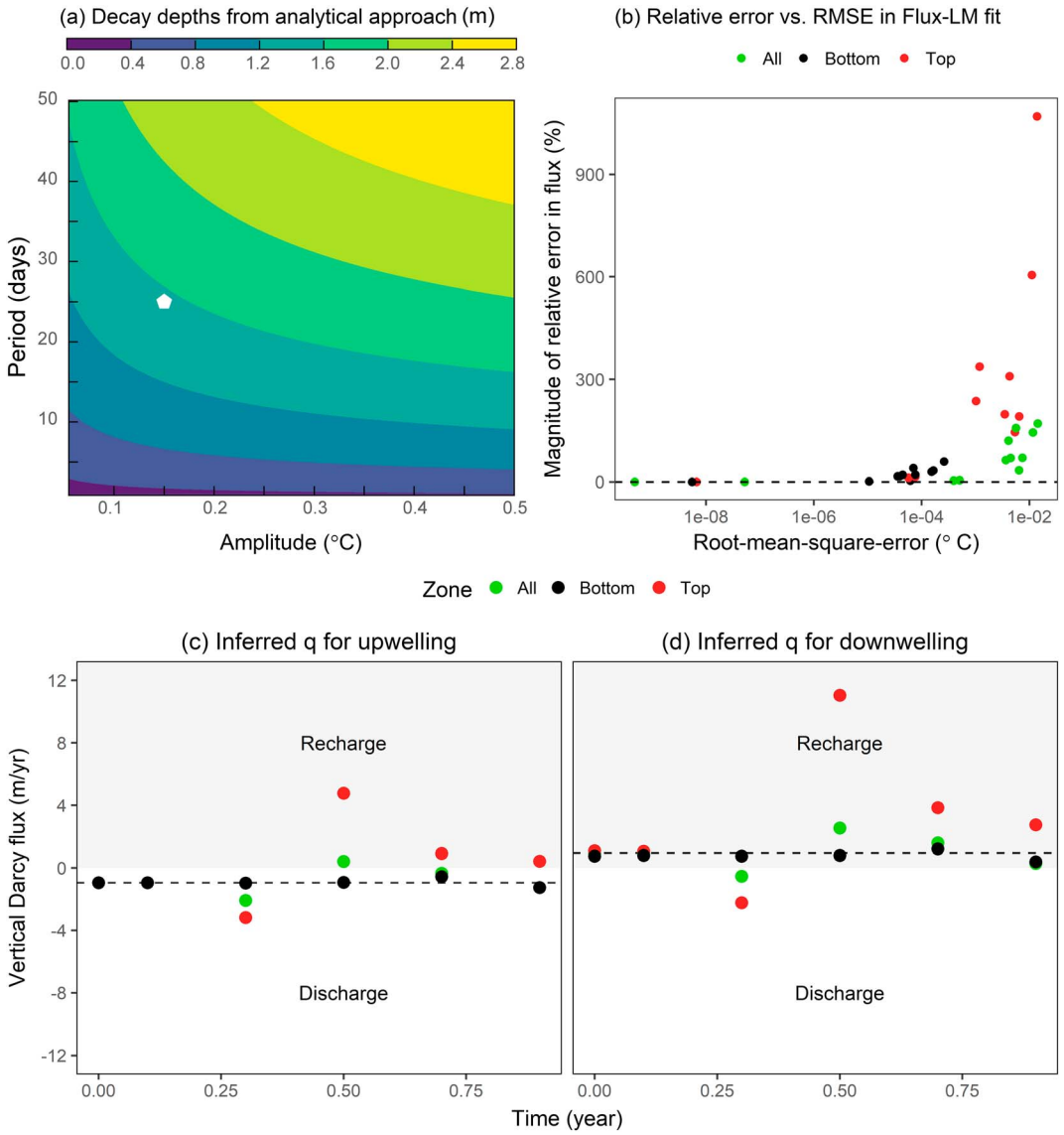

Figure 5. (a) BWT signal decay depths calculated with equation (2) for conditions representative of the study site (λ = 1.0 W · m · °C and $q = -1$ m/yr) for a range of periods and amplitudes. The white symbol denotes the decay depth for the highest amplitude (0.15 °C) and longest period (25 days) obtained from the SSD series in Figure 4a. Results were not very sensitive to the flux magnitude or direction within the limits of the fluxes inferred in this study. (b) Magnitude of *E* (equation (6)) versus the RMSE in the steady state fit to the FAST profiles. (c and d) Inferred Darcy fluxes from the steady state analyses for the entire profile ("all"), the bottom zone, and the top zone for the upwelling (c) and downwelling (d) profiles shown in Figures 4c and 4d. Light gray shading indicates recharge, while a white background indicates discharge. The dashed horizontal lines denote the actual fluxes used in the FAST modeling.

inferred flux, while the RMSE indicates the ability of the steady state function to match the transient temperature profiles. Figure 5b indicates that profiles with high *E* values were also characterized by relatively high RMSE values. This is important to note because it indicates that the RMSE values, which can always be quantified, may be useful as a proxy for the *E* values, which would typically be unknown when analyzing field data without alternative *q* measurements.

Figures 5c and 5d present the actual fluxes used in the FAST modeling (dashed lines) and the estimated Darcy fluxes from the Bredehoeft and Papadopulos (1965) solution applied to the entire profile, bottom zone, and top zone. The shaded zones in these figure panels delineate the vertical flux directions. Points lying in the light gray zone for the upwelling run (Figure 5c) or white zone for the downwelling run (Figure 5d)

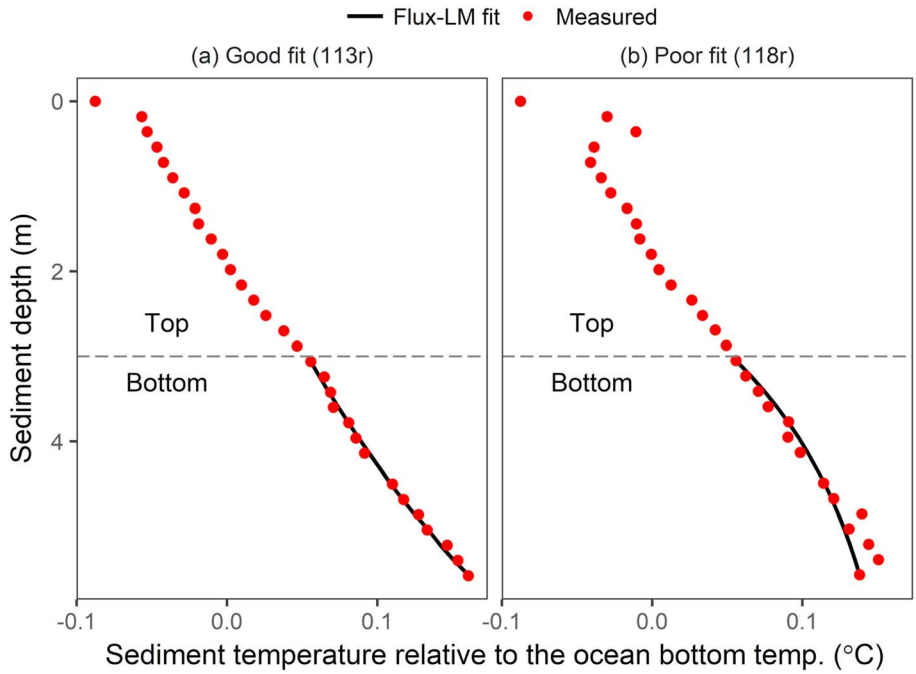

Figure 6. Examples of the Flux-LM fits (black line) to the measured data (red points) for the bottom part of the profiles. Most fits, such as that shown in (a) for profile 113r (q = 1.3 m/yr, RMSE = 0.0021 °C) had low RMSE values. (b) An example of a poor fit is presented for measured profile 118r (q = −4.0 m/yr, RMSE = 0.0075 °C). Temperatures are relative to the BWT.

indicate estimated fluxes that were in the wrong direction. The steady state analyses of the bottom zone profiles yielded fluxes that were close to the true magnitude and always in the correct direction.

4.3. Steady State, Homogeneous Analysis of the Bottom Zone Field Data

The above results indicate that temperature data below 3 m (bottom zone) outputted from the FAST modeling and driven by measured BWT variations on the Scotian Slope could be reasonably assessed using steady state methods (Figure 5). Thus, we applied these methods to infer fluxes from the bottom zone of the measured Scotian Slope temperature profiles. Figure 6, which presents two of these measured profiles, indicates that the sediment temperature profiles are not vertical like the temperature profile in the ocean bottom mixed layer. Flux-LM was used to process each of the 40 profiles with the Bredehoeft and Papadopulos (1965) equation. Generally, the fits to the bottom zone data were good (defined herein as RMSE $<$0.005 °C), with an overall average RMSE value of 0.0034 °C (e.g., Figure 6a). However, in five cases, the RMSE exceeded 0.005 °C (e.g., Figure 6b), indicating a poor fit. Relatively high RMSE values often occurred when the estimated q values had high magnitudes ($>$2 m/yr), but this was not always the case (Figure 7b). These high q values are uncertain because, as previously noted, high RMSE values are indicative that the error in the inferred flux (E, equation (6)) is also high (Figure 5b). For the five poor fits, the RMSE values could be lowered by allowing the bottom zone temperature to be adjusted during the optimization process in Flux-LM; however, we preferred to minimize the degrees of freedom and only adjust the Darcy flux during optimization. The RMSE values in the field data were always high compared to the RMSE values in the idealized FAST-modeled data, but this is expected given the field data scatter due to thermistor accuracy/resolution and potential issues during data collection and calibration. Also, the curvature in the field data appears to be minimal even at Darcy fluxes of 1 m/yr (Figure 6a). However, this is partly due to the small depth range (L ~ 3 m) considered in the present study compared to the much larger L values considered in more standard terrestrial applications of this method in deep aquifers (Irvine et al., 2016). Profile curvature in small-scale streambed applications of this technique can also be very hard to discern (Caissie et al., 2014). In general, the visual degree of curvature depends in part on the depth, temperature ranges, and aspect ratio presented on a plot.

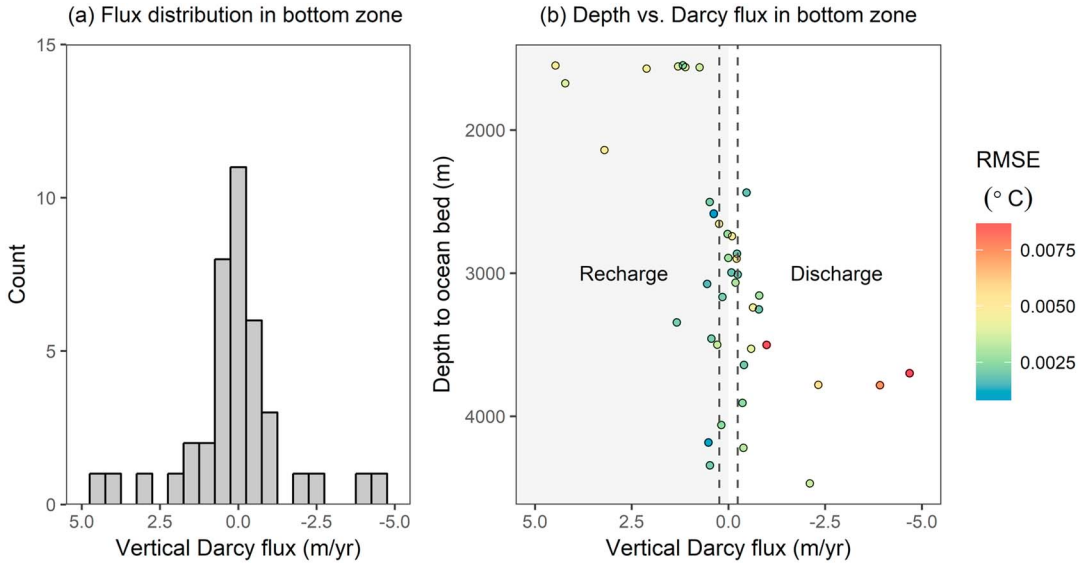

Figure 7. (a) Distribution of fluxes estimated via equation (5) for the bottom zone of the measured profiles. (b) Plot of inferred fluxes and ocean depths for the bottom zone with colors indicating the RMSE values. The shaded gray area indicates recharge, while the white background indicates discharge. The dashed vertical lines denote the locations of the minimum detectable flux magnitudes (equation (9)).

4.4. Steady State Heterogeneous Analysis of the Bottom Zone Field Data

The multilayered solution in Flux-LM (Kurylyk et al., 2017; Shan & Bodvarsson, 2004) was also applied to investigate the role of thermal conductivity variation on the estimated fluxes. The mean and standard deviations of the profile thermal conductivities were calculated and shown to be on average 1.07 and 0.14 ($W \cdot m^{-1} \cdot °C^{-1}$), respectively. These are presented in supporting information Figure S4. Furthermore, the thermal conductivity values were plotted versus depth for each profile, and these conductivity-depth profiles exhibited no discrete, sustained shifts indicative of multilayered sediment systems (e.g., Kurylyk et al., 2017). Rather, the thermal conductivity-depth profiles exhibited more oscillatory fluctuations (Figure S5) that are likely in part an artifact of the data collection process as the probe is known to smear the sediment during installation and also may retain water-filled voids larger than the sediment porosity. Both processes can create small artificial variation in the thermal properties, and as such, these minor oscillations likely indicate fluctuations due to the method accuracy and resolution. Nonetheless, simple multilayered steady state analyses were conducted in Flux-LM for a particularly heterogeneous profile (location 313, Negulic & Louden, 2017) with one-, two-, and three-layer scenarios to investigate what role thermal conductivity variation might have on the thermal profile curvature and estimated fluxes (Figure S5).

Even for this especially heterogeneous illustrative example, the inferred flux values were all generally close (within 21% Figure S5), regardless of how the thermal conductivity distribution was apportioned into discrete layers. Not accounting for thermal conductivity heterogeneity effects on the profile curvature can potentially yield incorrect flux magnitudes and direction; however, these results have only been found with discrete shifts in thermal conductivity on the order of 100 to 400% (Kurylyk et al., 2017). This only occurs with distinct layering. The present study had only minor measured thermal conductivity variations that were at least an order of magnitude smaller than in this previous study. In general, thermal conductivity variations are not considered to be a major source of profile curvature in the present study. Further details on the influence of thermal conductivity variations on inferred Darcy fluxes can be found in Kurylyk et al. (2017).

4.5. Submarine Groundwater Flow System

Given that the measured bottom zone temperature profiles are not expected to be greatly influenced by BWT variations (section 4.2) or thermal conductivity variations (section 4.4), the analysis conducted via the simple Bredehoeft and Papadopulos (1965) solution for the entire data set of thermal profiles (section 4.3) can be considered to gain insight into the regional submarine groundwater flow system on the Scotian Slope. Figure 7 presents the distribution of Darcy fluxes estimated via equation (5) for the bottom zone of the 40

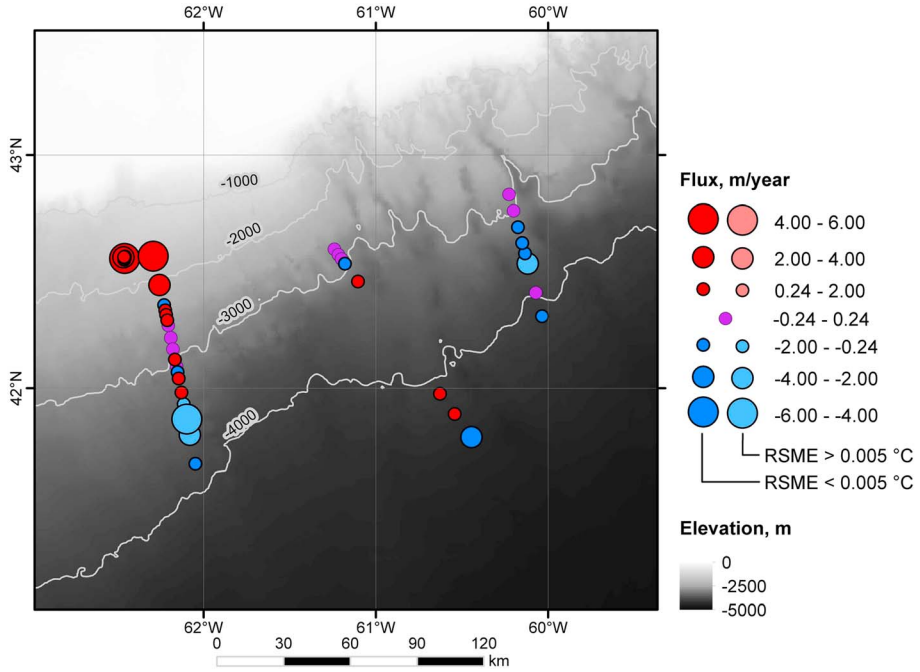

Figure 8. Map of inferred Darcy flux magnitudes (size) and directions (colors) overlaid on the elevation of the seabed. Red indicates recharge, blue indicates discharge, and purple indicates that the inferred flux magnitude is less than the theoretical detectable limit for the instrument (see equation (9)). Higher-magnitude fluxes can be exaggerative as discussed in section 4.3. The RMSE values for the model fits to the data are classified into high (RMSE >0.005 °C, light red and blue fill) values indicating a poor fit and low (RMSE <0.005 °C, dark red and blue fill) values indicating a better fit.

measured temperature profiles. A few profiles yielded high magnitude fluxes (e.g., 4 m/yr), but as previously discussed, these were also sometimes characterized by high RMSE values that indicate that the magnitudes are likely too high (see color, Figure 7b). Nonetheless, we would note that unlike terrestrial systems, there is an unlimited reservoir for groundwater recharge and K is likely higher in locations along the Scotian Slope than in many previously studied submarine hydrogeological settings (e.g., Abbott et al., 1981). The maximum SGD flux magnitudes are in the range of values directly measured using flux meters (e.g., up to 4 m/yr; Tryon et al., 2001). The hydraulic gradients required to transmit these flow rates would approach or even exceed 1, which is quite high for typical groundwater-surface water porous media interfaces (Rosenberry et al., 2015) based on the average of the K assumed across the study site. However, the site-to-site variation in the grain size distribution (Figure S1) and the coarse-scale surficial mapping by Piper and Campbell (2002) suggest that higher-K lenses are distributed throughout the slope, through which preferential SGD could occur at much lower hydraulic gradients.

Figure 7b shows the relationship between the ocean depths and Darcy fluxes inferred from the bottom zone of the Scotian Slope temperature profiles. Our temperature-based modeling results suggest that high groundwater recharge rates generally occur on the upper part of the slope (small ocean depths), whereas high discharge rates (negative fluxes) occur on its lower part (large ocean depths). For example, a linear model generated in R (R Core Team, 2017) between the inferred flux and the ocean depth data shown in Figure 7b yielded a negative slope and P and R^2 values of 1.1×10^{-5} and 0.41, respectively. If the linear model is weighted by the inverse of the RMSE to remove any strong influence from the more uncertain higher flux points, the linear model still yields a negative slope and a statistically significant relationship ($P = 6.0 \times 10^{-4}$, $R^2 = 0.27$). These simple statistical results do not imply that there is a linear causal relationship between flux and depth, but they do at least suggest a pattern. This relationship can also be seen when the inferred flux distribution is overlaid on a bathymetry map (see colors and symbol sizes, Figure 8).

The driving mechanisms for this inferred groundwater flow system have not been addressed in the quantitative analyses in this study. However, we briefly speculate on these processes here. Others (see Figure 1 of Wilson, 2005) have proposed that bathymetrically driven systems, with recharge and discharge

respectively at high and low seabed elevations, similar to Figure 8, can occur in continental shelves. However, groundwater flow systems in continental slopes are classically thought to be driven by geothermal convection, which creates upward flow through the slope (Kohout, 1965). This "Kohout convection" has been shown for carbonate platforms (e.g., Jones & Xiao, 2006) that are distinct from the geology of the Scotian Slope (section 2.1). Furthermore, there are known underlying salt domes in the slope (Negulic & Louden, 2017), and salt domes cause a region of high-salinity and dense water around them (Evans et al., 1991). In deep marine environments, downward groundwater flow strongly suggests density-related convection (Wilson & Ruppel, 2007), and different mechanisms for density-driven convection due to high salinity brines have been proposed (Evans et al., 1991; Sharp Jr. et al., 2001; Stover et al., 2001a, 2001b). In general, dense brines can sink and draw water from above, causing a downward flow system such as that seen on the Scotian Slope. Convective SGD patterns can be caused by underlying salt domes far beneath the seabed even in the absence of faults or fracture networks connecting the seabed surface and the salt dome, but flow rates can increase considerably when such networks are present (Wilson & Ruppel, 2007). Geophysical surveys along Line 1 of the Scotian Slope clearly indicate faults located above the salt domes (Negulic & Louden, 2017) that could mediate flow depending on their connection to the surface (Bense et al., 2013). However, we acknowledge that these process-based explanations are speculative and that more data and conceptual modeling are needed. We also acknowledge that the flux distribution in Figure 8 may be the result of local, density-driven circulation cells, rather than a slope-driven system.

More submarine hydrogeology research has been conducted on continental shelves in comparison to continental slopes due to all of the continental shelf oil and gas exploration and associated drilling (e.g., Bratton, 2010; Hughes et al., 2009; Thompson et al., 2007; Wilson, 2003). Further hydrogeological research is warranted to draw more concrete conclusions on the Scotian Slope given the noted uncertainties in the steady state, homogeneous heat tracing approach used to generate the results shown in Figures 7b and 8. In particular, the potential for the large salt domes, or more generally salinity variations, to induce density-driven submarine groundwater flow (Evans et al., 1991; Michael et al., 2016; Wilson & Ruppel, 2007) and the influence of the fault and fracture network in the Scotian Slope (Negulic & Louden, 2017) will be investigated in future numerical modeling studies of coupled groundwater flow and heat and solute transport. Given the distance from the continent and the delineated recharge zones along the slope crest (Figure 8), it is unlikely that the SGD toward the lower Scotian Slope is fresh. However, even saline SGD circulation can impact seabed and deep-ocean biogeochemistry (Zektser & Dzhamalov, 2007).

5. Study Considerations

5.1. Temporal Considerations for Data Collection and Appropriate Method Application

The present study has demonstrated that transient and steady state heat tracing techniques may be used in concert to estimate submarine groundwater flow rates from temperature profiles collected in deep-ocean sediment. If BWT data distributed across the study site are recorded prior to the collection of the temperature profiles and if sediment temperature time series are available, transient methods can be directly applied to infer groundwater fluxes. BWT sensors should be installed at least several months prior to the thermal profile measurements to characterize the frequency spectrum of the variations. However, continuous seabed temperature data would be logistically difficult to obtain in deep marine settings as it would be prohibitively expensive to install probes semipermanently at each location rather than use a single probe to record each profile. Furthermore, collecting repeat profiles, rather than a continuous time series, can yield insight into groundwater fluxes (Bense et al., 2017; Bense & Kurylyk, 2017) but this is challenging in deep marine environments due to difficulties with driving the probe into identical or very nearby locations.

If, as in the present study, BWT data are available with only "snapshots" of the sediment thermal profile measurements, transient approaches can be applied to delineate steady state and transient zones. If the BWT is constant, then steady state methods can be applied across the entire profile. In general, either homogeneous (Bredehoeft & Papadopulos, 1965) or multilayer (Shan & Bodvarsson, 2004) steady state methods can be employed depending on whether the thermal conductivity profile obtained from the heat pulse decay exhibits pronounced heterogeneity. If the domain is both transient and heterogeneous, a numerical thermal tracing model should be employed (Koch et al., 2016; Munz & Schmidt, 2017; Wilson et al., 2016). Options for using ocean sediment temperature profiles to trace submarine groundwater flow based on the timescale of data availability are shown in Figure 3.

5.2. Spatial and Accuracy Considerations for Data Collection and Flux Detection Limits

The depths and accuracy of the seabed probe's thermistor readings strongly influence the utility and flux detection limits of the methods applied in this study. The profile must be long enough such that the curvature deviation from a linear profile can be determined for curve fitting using the Bredehoeft and Papadopulos (1965) approach. This deviation (Δ, °C) should then be compared to the thermal sensor accuracy to determine if modeled fluxes can confidently be classified as significantly different than zero (a linear thermal gradient). The deviation can be calculated as the difference between the Bredehoeft and Papadopulos (1965) solution and a linear profile:

$$\Delta = (T_L - T_0)\left[\frac{\exp(\beta z/L) - 1}{\exp(\beta) - 1} - \frac{z}{L}\right] \tag{7}$$

Equating the derivative of equation (7) to 0 to yield the local maximum or minimum and then rearranging to isolate the depth ($z_{\Delta max}$, m) at which the maximum positive or negative deviation (Δ_{max}, °C) occurs results in equation (8).

$$z_{\Delta\,max} = \ln\left\{\frac{\exp(\beta) - 1}{\beta}\right\}\frac{L}{\beta} \tag{8}$$

Inserting equation (8) into equation (7) enables the calculation of maximum deviation Δ_{max}.

$$\Delta_{max} = (T_L - T_0)\left\{\frac{\exp(\beta) - 1 - \beta}{\beta\exp(\beta) - \beta} - 1n\left[\frac{\exp(\beta) - 1}{\beta}\right]\frac{1}{\beta}\right\} \tag{9}$$

Equation (9) can be used to obtain an appropriate L and/or sensor accuracy based on the possible Darcy flux range and thermal properties. In general, thermal probes that extend to depths greater than 6 m should be employed if possible. For example, some seabed thermal probes extend to 10 m (Davis & Elderfield, 2004). The probe used to collect the data in this study was almost 6-m long, and having an additional 4 m would more than double the length of the profile that could be analyzed using steady state approaches. For the present study conditions, the magnitude of Δ_{max} obtained from equation (9) is approximately 0.0042 °C for a q of 1 m/yr and 0.016 °C for a q of 4 m/yr, but these values would respectively increase to 0.011 °C and 0.045 °C if L were increased to 7 m.

Equation (9) also demonstrates that the flux detection limits are influenced by the sensor accuracy. For example, thermistors with a realized accuracy of ±0.01 °C would not be useful for the quantification of a q of a 1 m/yr (deviation of 0.005 °C) over a 3-m profile, but the same sensors could be used to identify (if not quantify) this same flux using a 7-m profile (deviation of 0.011 °C). In this study high-accuracy sensors were used (0.001 °C), hypothetically allowing the identification of vertical fluxes with magnitudes greater than 0.24 m/yr. The vertical dashed lines in Figure 7b indicate that 10 of the 40 profiles exhibit insufficient curvature to conclusively identify a flux. It should also be noted that thermistors with very high precision but low accuracy could potentially produce artificial profile curvature that could be falsely attributed to vertical fluid fluxes. In the present study, the precision was equivalent to the accuracy.

6. Summary and Conclusions

Forty thermal profiles collected in deep-ocean sediment of the Scotian Slope off the eastern coast of Canada were analyzed to estimate rates of submarine groundwater exchange. Transient heat tracing techniques recently developed for terrestrial environments, but not previously employed in marine settings, were applied to consider the thermal interplay among bottom water temperature changes, thermal conductivity variation, and vertical groundwater flow. Transient thermal modeling indicated that BWT changes caused intra-annual variations (and thus transience-induced curvature) in the sediment temperature profiles, but this intra-annual temperature variability decayed with depth and was very minimal below depths of 3 m. Thus, the portions of each temperature profile extending below 3 m were analyzed using steady state methods. The spatial distribution of submarine groundwater fluxes inferred from this analysis tentatively suggests a submarine groundwater flow system that is recharged over the upper slope and discharges toward the

lower slope. This downward flow is different from upward, continental slope flow systems driven by geothermal convection that have been proposed in the literature. We speculate that the inferred groundwater flow system may be due to density-driven flow induced by underlying salt domes. Detailed numerical modeling of groundwater flow and heat transport in the Scotian Scope will be conducted in the future to investigate these hypotheses.

The new techniques applied in this study have potential to be used at many other deep-ocean sites where sediment temperature profiles are available. The influence of BWT variation can be addressed by either using a transient approach to delineate the upper surface of the steady state zone or, when sediment temperature time series are available, directly applying a transient heat tracing technique to back out fluxes. Future field campaigns that collect seabed thermal data for hydrogeological purposes should consider longer probes with sensor placement dependent on the intended analysis for heat tracing (steady state or transient). In general, we call for more submarine hydrogeological research to be conducted in deep marine environments. Additional physical and chemical methodologies to complement thermal methods in deep offshore environments will be critical to elucidating mechanisms driving deep-submarine groundwater flow and to assess intersite variations in flow system characteristics and the influence on the biogeochemistry of deep-ocean benthic environments.

Acknowledgments
Keith Louden (Dalhousie University) is thanked for kindly sharing the ocean sediment thermal data and providing invaluable advice. Calvin Campbell (Geological Survey of Canada) graciously provided general information on the surficial geology of the Scotian Basin and directed us to the sediment grain size analysis data for the area. Igor Pavlovskii (University of Calgary) is thanked for his assistance in creating the maps. Technical and vessel personnel at the Bedford Institute of Oceanography are thanked for their execution of the moored BWT measurement program, which was funded by Fisheries and Oceans Canada and the (Canadian) Federal Program of Energy Research and Development. Alicia Wilson, Grant Ferguson, and two anonymous reviewers and an Associate Editor provided helpful comments that improved this study. Any use of trade, firm, or product names is for descriptive purposes only and does not imply endorsement by the U.S. Government. The raw data for this study were previously reported in the cited Negulic and Louden (2017) study and are not included in the Supplementary Information. However, we do include the model data used to generate the figures in the present study. Figure S1 shows the grain size distributions for the seabed sediment samples taken in the region of study. Figure S2 shows results of the 2-D steady state thermal modeling to investigate the influence of the slope on the temperature distribution. Table S1 and Figure S3 present the initial conditions for the FAST modeling. Figure S4 shows the thermal conductivity data for each profile. Figure S5 shows the Flux-LM results when the seabed sediment was treated as multilayer, heterogeneous systems. Table S2 contains tabulated values for the inferred fluxes for the bottom zone for each analyzed profile, including the depths and coordinates for each location. This information is embedded in Figures 1b, 6, 7, and 8. Table S3 contains the raw temperature-depth output from the FAST analysis used to delineate the "top" and "bottom" zones (Figures 4 and 5). The FAST Python code is included as a supplement to Kurylyk and Irvine (2016), and the Flux-LM spreadsheet tool is included as a supplement to Kurylyk et al. (2017).

References

Abbott, D., Menke, W., Hobart, M., & Anderson, R. (1981). Evidence for excess pore pressures in southwest Indian Ocean sediments. *Journal of Geophysical Research*, *86*(B3), 1813–1827. https://doi.org/10.1029/JB086iB03p01813

Anderson, M. P. (2005). Heat as a ground water tracer. *Ground Water*, *43*(6), 951–968. https://doi.org/10.1111/j.1745-6584.2005.00052.x

Anderson, R. N., Hobart, M. A., & Langseth, M. G. (1979). Geothermal convection through oceanic crust and sediments in the Indian Ocean. *Science*, *204*(4395), 828–832. https://doi.org/10.1126/science.204.4395.828

Armi, L., & Millard, R. C. (1976). The bottom boundary layer of the deep ocean. *Journal of Geophysical Research*, *81*(27), 4983–4990. https://doi.org/10.1029/JC081i027p04983

Befus, K. M., Cardenas, M. B., Erler, D. V., Santos, I. R., & Eyre, B. D. (2013). Heat transport dynamics at a sandy intertidal zone. *Water Resources Research*, *49*, 3770–3786. https://doi.org/10.1002/wrcr.20325

Bense, V. F., Gleeson, T., Loveless, S. E., Bour, O., & Scibek, J. (2013). Fault zone hydrogeology. *Earth-Science Reviews*, *127*, 171–192. https://doi.org/10.1016/j.earscirev.2013.09.008

Bense, V. F., & Kooi, H. (2004). Temporal and spatial variations of shallow subsurface temperature as a record of lateral variations in groundwater flow. *Journal of Geophysical Research*, *109*, B04103. https://doi.org/10.1029/2003JB002782

Bense, V. F., & Kurylyk, B. L. (2017). Tracking the subsurface signal of decadal climate warming to quantify vertical groundwater flow rates. *Geophysical Research Letters*, *44*, 12,244–12,253. https://doi.org/10.1002/2017GL076015

Bense, V. F., Kurylyk, B. L., van Daal, J., van der Ploeg, M., & Carey, S. K. (2017). Interpreting repeated temperature-depth profiles for groundwater flow. *Water Resources Research*, *53*, 8639–8647. https://doi.org/10.1002/2017WR021496

Beusen, A. H. W., Slomp, C. P., & Bouwman, A. F. (2013). Global land–ocean linkage: Direct inputs of nitrogen to coastal waters via submarine groundwater discharge. *Environmental Research Letters*, *8*(3), 34035. https://doi.org/10.1088/1748-9326/8/3/034035

Bratton, J. F. (2010). The three scales of submarine groundwater flow and discharge across passive continental margins. *Journal of Geology*, *118*(5), 565–575. https://doi.org/10.1086/655114

Bredehoeft, J. D., & Papadopulos, I. S. (1965). Rates of vertical groundwater movement estimated from the Earth's thermal profile. *Water Resources Research*, *1*(2), 325–328. https://doi.org/10.1029/WR001i002p00325

Briggs, M. A., Lautz, L. K., Buckley, S. F., & Lane, J. W. (2014). Practical limitation on the use of diurnal temperature signals to quantify groundwater upwelling. *Journal of Hydrology*, *519*, 1739–1751. https://doi.org/10.1016/j.jhydrol. 2014.09.030

Bullard, E. (1954). The flow of heat through the floor of the Atlantic Ocean. *Proceedings of the Royal Society of London. Series A: Mathematical and Physical Sciences*, *222*(1150), 408–429. https://doi.org/10.1098/rspa.1954.0085

Burnett, W. C., Aggarwal, P. K., Aureli, A., Bokuniewicz, H., Cable, J. E., Charette, M. A., et al. (2006). Quantifying submarine groundwater discharge in the coastal zone via multiple methods. *Science of the Total Environment*, *367*(2-3), 498–543. https://doi.org/10.1016/j.scitotenv. 2006.05.009

Burnett, W. C., Bokuniewicz, H., Huettel, M., Moore, W. S., & Taniguchi, M. (2003). Groundwater and pore water inputs to the coastal zone. *Biogeochemistry*, *66*(1/2), 3–33. https://doi.org/10.1023/B:BIOG.0000006066.21240.53

Caissie, D., Kurylyk, B. L., St-Hilaire, A., El-Jabi, N., & MacQuarrie, K. T. B. (2014). Streambed temperature dynamics and corresponding heat fluxes in small streams experiencing seasonal ice cover. *Journal of Hydrology*, *519*, 1441–1452. https://doi.org/10.1016/j.jhydrol.2014.09.034

Davis, E., & Elderfield, H. (2004). *Hydrogeology of the oceanic lithosphere*. Cambridge, UK: Cambridge University Press.

Davis, E. E., Lister, C. R. B., & Sclater, J. G. (1984). Towards determining the thermal state of old ocean lithosphere: Heat-flow measurements from the Blake–Bahama outer ridge, north-western Atlantic. *Geophysical Journal of the Royal Astronomical Society*, *78*(2), 507–545. https://doi.org/10.1111/j.1365-246X.1984.tb01962.x

Davis, E. E., Wang, K., Becker, K., Thomson, R. E., & Yashayaev, I. (2003). Deep-ocean temperature variations and implications for errors in seafloor heat flow determinations. *Journal of Geophysical Research*, *108*(B1), 2034. https://doi.org/10.1029/2001JB001695

Evans, D. G., Nunn, J. A., & Hanor, J. S. (1991). Mechanisms driving groundwater flow near salt domes. *Geophysical Research Letters*, *18*(5), 927–930. https://doi.org/10.1029/91GL00908

Fetter, C. W. (2001). *Applied hydrogeology* (4th ed.). Upper Saddle River, New Jersey: Prentice-Hall, Inc.

Fisher, A. T. (2004). Rates of flow and patterns of fluid circulation. In E. Davis, & H. Enderfield (Eds.), *Hydrogeology of the oceanic lithosphere* (pp. 337–376). Cambridge, UK: Cambridge University Press.

Fisher, A. T., & Becker, K. (1991). Heat flow, hydrothermal circulation and basalt intrusions in the Guaymas Basin, Gulf of California. *Earth and Planetary Science Letters*, *103*(1-4), 84–99. https://doi.org/10.1016/0012-821X(91)90152-8

Fukasawa, M., Freeland, H., Perkin, R., Watanabe, T., Uchida, H., & Nishina, A. (2004). Bottom water warming in the North Pacific Ocean. *Nature*, *427*(6977), 825–827. https://doi.org/10.1038/nature02337

Geller, C. A., Weissel, J. K., & Anderson, R. N. (1983). Heat transfer and intraplate deformation in the central Indian Ocean. *Journal of Geophysical Research*, *88*(B2), 1018–1032. https://doi.org/10.1029/JB088iB02p01018

Geological Survey of Canada (2017). Natural resources Canada grain size database. Retrieved from http://ed.gdr.nrcan.gc.ca/grainsize_e.php

Goto, S., Yamano, M., & Kinoshita, M. (2005). Thermal response of sediment with vertical fluid flow to periodic temperature variation at the surface. *Journal of Geophysical Research*, *110*, B01106. https://doi.org/10.1029/2004JB003419

Harris, R. N., & Chapman, D. S. (1995). Climate change on the Colorado Plateau of eastern Utah inferred from borehole temperatures. *Journal of Geophysical Research*, *100*(B4), 6367–6381. https://doi.org/10.1029/94JB02165

Harris, R. N., & Higgins, S. M. (2008). A permeability estimate in 56 Ma crust at ODP Hole 642E, Vøring plateau Norwegian Sea. *Earth and Planetary Science Letters*, *267*(1–2), 378–385. https://doi.org/10.1016/j.epsl.2007.11.055

Harris, R. N., & the IODP Expedition 306 Scientists (2006). Borehole observatory installations on IODP expedition 306 reconstruct bottom-water temperature changes in the Norwegian Sea. *Scientific Drilling*, *2*, 28–31. https://doi.org/10.5194/sd-2-28-2006

Hatch, C. E., Fisher, A. T., Revenaugh, J. S., Constantz, J., & Ruehl, C. (2006). Quantifying surface water-groundwater interactions using time series analysis of streambed thermal records: Method development. *Water Resources Research*, *42*, W10410. https://doi.org/10.1029/2005WR004787

Heiss, J. W., & Michael, H. A. (2014). Saltwater-freshwater mixing dynamics in a sandy beach aquifer over tidal, spring-neap, and seasonal cycles. *Water Resources Research*, *50*, 6747–6766. https://doi.org/10.1002/2014WR015574

Hughes, J. D., Vacher, H. L., & Sanford, W. E. (2009). Temporal response of hydraulic head, temperature, and chloride concentrations to sea-level changes, Floridan aquifer system, USA. *Hydrogeology Journal*, *17*(4), 793–815. https://doi.org/10.1007/s10040-008-0412-0

Irvine, D. J., Cartwright, I., Post, V. E. A., Simmons, C. T., & Banks, E. W. (2016). Uncertainties in vertical groundwater fluxes from 1-D steady state heat transport analyses caused by heterogeneity, multidimensional flow, and climate change. *Water Resources Research*, *52*, 813–826. https://doi.org/10.1002/2015WR017702

Irvine, D. J., Kurylyk, B. L., Cartwright, I., Bonham, M., Post, V. E. A., Banks, E. W., & Simmons, C. T. (2017). Groundwater flow estimation using temperature-depth profiles in a complex environment and a changing climate. *Science of the Total Environment*, *574*, 272–281. https://doi.org/10.1016/j.scitotenv.2016.08.212

Jansa, L. F., & Wade, J. A. (1975). Geology of the continental margin of Nova Scotia and Newfoundland. In W. J. M. van der Linden & J. A. Wade (Eds.), *Offshore geology of eastern Canada Vol*. 2 (51–106). Geological Survey of Canada.

Johannes, R. E. (1980). The ecological significance of the submarine discharge of groundwater. *Marine Ecology Progress Series*, *3*, 365–373. https://doi.org/10.3354/meps003365

Johnson, G. C., Mecking, S., Sloyan, B. M., & Wijffels, S. E. (2007). Recent bottom water warming in the Pacific Ocean. *Journal of Climate*, *20*(21), 5365–5375. https://doi.org/10.1175/2007JCLI1879.1

Jones, G. D., & Xiao, Y. (2006). Geothermal convection in the Tengiz carbonate platform, Kazakhstan: Reactive transport models of diagenesis and reservoir quality. *American Association of Petroleum Geologists*, *90*(8), 1251–1272. http://doi.org/10.1306/04030605194

Kazemi, G. A. (2008). Editor's message: Submarine groundwater discharge studies and the absence of hydrogeologists. *Hydrogeology Journal*, *16*(2), 201–204. https://doi.org/10.1007/s10040-007-0251-4

Koch, F. W., Voytek, E. B., Day-Lewis, F. D., Healy, R., Briggs, M. A., Lane, J. W., & Werkema, D. (2016). 1DTempPro V2: New features for inferring groundwater/surface-water exchange. *Groundwater*, *54*(3), 434–439. https://doi.org/10.1111/gwat.12369

Kohout, F. A. (1965). A hypothesis concerning cyclic flow of salt water related to geothermal heating in the Floridan aquifer. *Transactions of the New York academy of science*, *28*(2 Series II), 249–271. https://doi.org/10.1111/j.2164-0947.1965.tb02879.x

Kuhn, T., Versteegh, G. J. M., Villinger, H., Dohrmann, I., Heller, C., Koschinsky, A., et al. (2017). Widespread seawater circulation in 18–22 Ma oceanic crust: Impact on heat flow and sediment geochemistry. *Geology*, *45*(9), 799–802. https://doi.org/10.1130/G39091.1

Kurylyk, B. L., & Irvine, D. J. (2016). Analytical solution and computer program (FAST) to estimate fluid fluxes from subsurface temperature profiles. *Water Resources Research*, *52*, 725–733. https://doi.org/10.1002/2015WR017990

Kurylyk, B. L., Irvine, D. J., Carey, S. K., Briggs, M. A., Werkema, D., & Bonham, M. (2017). Heat as a groundwater tracer in shallow and deep heterogeneous media: Analytical solution, spreadsheet tool, and field applications. *Hydrological Processes*, *31*(14), 2648–2661. https://doi.org/10.1002/hyp.11216

Kurylyk, B. L., & MacQuarrie, K. T. B. (2014). A new analytical solution for assessing climate change impacts on subsurface temperature. *Hydrological Processes*, *28*(7), 3161–3172. https://doi.org/10.1002/hyp.9861

Langseth, M. G., & Herman, B. M. (1981). Heat transfer in the oceanic crust of the Brazil Basin. *Journal of Geophysical Research*, *86*(B11), 10,805–10,819. https://doi.org/10.1029/JB086iB11p10805

Li, L., Barry, D. A., Stagnitti, F., & Parlange, J.-Y. (1999). Submarine groundwater discharge and associated chemical input to a coastal sea. *Water Resources Research*, *35*(11), 3253–3259. https://doi.org/10.1029/1999WR900189

Lister, C. R. B. (1979). The pulse-probe method of conductivity measurement. *Geophysical Journal of the Royal Astronomical Society*, *57*(2), 451–461. https://doi.org/10.1111/j.1365-246X.1979.tb04788.x

Louden, K. E., Sibuet, J.-C., & Harmegnies, F. (1997). Variations in heat flow across the ocean—Continent transition in the Iberia abyssal plain. *Earth and Planetary Science Letters*, *151*(3–4), 233–254. https://doi.org/10.1016/S0012-821X (97)81851-1

Louden, K. E., & Wright, J. A. (1989). Marine heat flow data: A new compilation of observations and brief review of its analysis. In J. A. Wright, & K. E. Louden (Eds.), *CRC handbook of seafloor heat flow* (pp. 3–72). Boca Raton, FL: CRC Press, Inc.

Luce, C. H., Tonina, D., Gariglio, F. P., & Applebee, R. (2013). Solutions for the diurnally forced advection-diffusion equation to estimate bulk fluid velocity and diffusivity in streambeds from temperature time series. *Water Resources Research*, *49*, 488–506. https://doi.org/10.1029/2012WR012380

Menberg, K., Blum, P., Kurylyk, B. L., & Bayer, P. (2014). Observed groundwater temperature response to recent climate change. *Hydrology and Earth System Sciences*, *18*(11), 4453–4466. https://doi.org/10.5194/hess-18-4453-2014

Michael, H. A., Mulligan, A. E., & Harvey, C. F. (2005). Seasonal oscillations in water exchange between aquifers and the coastal ocean. *Nature*, *436*(7054), 1145–1148. https://doi.org/10.1038/nature03935

Michael, H. A., Post, V. E. A., Wilson, A. M., & Werner, A. D. (2017). Science, society, and the coastal groundwater squeeze. *Water Resources Research*, *53*, 2610–2617. https://doi.org/10.1002/2017WR020851

Michael, H. A., Scott, K. C., Koneshloo, M., Yu, X., Khan, M. R., & Li, K. (2016). Geologic influence on groundwater salinity drives large seawater circulation through the continental shelf. *Geophysical Research Letters*, *43*, 10,782–10,791. https://doi.org/10.1002/2016GL070863

Moore, W. S. (2010). The effect of submarine groundwater discharge on the ocean. *Annual Review of Marine Science*, *2*(1), 59–88. https://doi.org/10.1146/annurev-marine-120308-081019

Munz, M., & Schmidt, C. (2017). Estimation of vertical water fluxes from temperature time series by the inverse numerical computer program FLUX-BOT. *Hydrological Processes*, *31*(15), 2,713–2,724. https://doi.org/10.1002/hyp.11198

Negulic, E., & Louden, K. E. (2017). The thermal structure of the central Nova Scotia Slope (eastern Canada): Seafloor heat flow and thermal maturation models. *Canadian Journal of Earth Sciences*, *54*(2), 146–162. https://doi.org/10.1139/cjes-2016-0060

Negulic, E. W. (2010). Thermal structure of the central Scotian Slope: Seafloor heat flow and thermal maturation models. MSc Thesis, Dalhousie University, Halifax, Canada. Retrieved from https://dalspace.library.dal.ca/handle/10222/13134

Noel, M. (1984). Origins and significance of non-linear temperature profiles in deep-sea sediments. *Geophysical Journal of the Royal Astronomical Society*, *76*(3), 673–690. https://doi.org/10.1111/j.1365-246X.1984.tb01916.x

Peña-Molino, B., Joyce, T. M., & Toole, J. M. (2012). Variability in the deep western boundary current: Local versus remote forcing. *Journal of Geophysical Research*, *117*, C12022. https://doi.org/10.1029/2012JC008369

Piper, D. J. W., & Campbell, D. C. (2002). Surficial geology of the Scotian Slope, Eastern Canada. Geological Survey of Canada Report # 2002-E15. Retrieved from http://publications.gc.ca/Collections/collection_2007/nrcan-rncan/M44–2002-E15E.pdf

Post, V. E. A., Groen, J., Kooi, H., Person, M., Ge, S., & Edmunds, W. M. (2013). Offshore fresh groundwater reserves as a global phenomenon. *Nature*, *504*(7478), 71–78. https://doi.org/10.1038/nature12858

R Core Team (2017). *R: A language and environment for statistical computing*. Vienna, Austria: R Foundation for Statistical Computing. URL https://www.r-project.org/

Rau, G., Anderson, M. S., McCallum, A. M., Roshan, H., & Acworth, R. I. (2014). Heat as a tracer to quantify water flow in near-surface sediments. *Earth-Science Reviews*, *129*, 40–58. https://doi.org/10.1016/j.earscirev.2013.10.015

Reiter, M. (2005). Possible ambiguities in subsurface temperature logs: Consideration of ground-water flow and ground surface temperature change. *Pure and Applied Geophysics*, *162*(2), 343–355. https://doi.org/10.1007/s00024-004-2604-4

Robinson, C., Li, L., & Barry, D. A. (2007). Effect of tidal forcing on a subterranean estuary. *Advances in Water Resources*, *30*(4), 851–865. https://doi.org/10.1016/j.advwatres.2006.07.006

Rosenberry, D. O., Lewandowski, J., Meinikmann, K., & Nützmann, G. (2015). Groundwater—The disregarded component in lake water and nutrient budgets. Part 1: Effects of groundwater on hydrology. *Hydrological Processes*, *29*(13), 2895–2921. https://doi.org/10.1002/hyp.10403

Saar, M. O. (2011). Review: Geothermal heat as a tracer of large-scale groundwater flow and as a means to determine permeability fields. *Hydrogeology Journal*, *19*(1), 31–52. https://doi.org/10.1007/s10040-010-0657-2

Santos, I. R., Bradley, B. D., & Huettel, M. (2012). The driving forces of porewater and groundwater flow in permeable coastal sediments: A review. *Estuarine, Coastal and Shelf Science*, *98*, 1–15. https://doi.org/10.1016/j.ecss. 2011.10.024

Sawyer, A. H., Michael, H. A., & Schroth, A. W. (2016). From soil to sea: The role of groundwater in coastal critical zone processes. *Wiley Interdisciplinary Reviews: Water*, *3*(5), 706–726. https://doi.org/10.1002/wat2.1157

Shan, C., & Bodvarsson, G. (2004). An analytical solution for estimating percolation rate by fitting temperature profiles in the vadose zone. *Journal of Contaminant Hydrology*, *68*(1–2), 83–95. https://doi.org/10.1016/S0169-7722(03)00126-8

Sharp, J. M. Jr., Fenstemaker, T. R., Simmons, C. T., McKenna, T. E., & Dickinson, J. K. (2001). Potential salinity-driven free convection in a shale-rich sedimentary basin: Example from the Gulf of Mexico basin in South Texas. *AAPG Bulletin*, *85*, 2089–2110.

Shaw, J., & Courtney, R. C. (2004). A digital elevation model of Atlantic Canada. Geological Survey of Canada Open File Report4634. https://doi.org/10.4095/215828

Slomp, C. P., & Van Cappellen, P. (2004). Nutrient inputs to the coastal ocean through submarine groundwater discharge: Controls and potential impact. *Journal of Hydrology*, *295*(1-4), 64–86. https://doi.org/10.1016/j.jhydrol.2004.02.018

Smith, J. N., Smethie, W. M., Yashayev, I., Curry, R., & Azetsu-Scott, K. (2016). Time series measurements of transient tracers and tracer-derived transport in the Deep Western Boundary Current between the Labrador Sea and the subtropical Atlantic Ocean at Line W. *Journal of Geophysical Research: Oceans*, *121*, 8,115–8,138. https://doi.org/10.1002/2016JC011759

Stallman, R. W. (1963). Methods of collecting and interpreting ground-water data. *U. S. Geological Survey Water-Supply Paper*, *1544–H*, 36–46.

Stallman, R. W. (1965). Steady one-dimensional fluid flow in a semi-infinite porous medium with sinusoidal surface temperature. *Journal of Geophysical Research*, *70*(12), 2,821–2,827. https://doi.org/10.1029/JZ070i012p02821

Stover, S. C., Ge, S., Weimer, P., & McBride, B. C. (2001b). The effects of salt evolution, structural development, and fault propagation on Late Mesozoic-Cenozoic oil migration: A two-dimensional fluid flow study along a megaregional profile in the northern Gulf of Mexico Basin. *AAPG Bulletin*, *85*, 1945–1966.

Stover, S. C., Weimer, P., & Ge, S. (2001a). The effect of allochthonous salt evolution and overpressure development on source rock thermal maturation: A two-dimensional transient study in the northern Gulf of Mexico Basin. *Petroleum Geoscience*, *7*(3), 281–290. https://doi.org/10.1144/petgeo.7.3.281

Taniguchi, M., Burnett, W. C., Cable, J. E., & Turner, J. V. (2002). Investigation of submarine groundwater discharge. *Hydrological Processes*, *16*(11), 2115–2129. https://doi.org/10.1002/hyp.1145

Taniguchi, M., Shimada, J., Tanaka, T., Kayane, I., Sakura, Y., Shimano, Y., et al. (1999). Disturbances of temperature-depth profiles due to surface climate change and subsurface water flow: 1. An effect of linear increase in surface temperature caused by global warming and urbanization in the Tokyo Metropolitan Area, Japan. *Water Resources Research*, *35*(5), 1507–1517. https://doi.org/10.1029/1999WR900009

The MathWorks, Inc. (2014). MATLAB and Statistics Toolbox Release Natick, Massachusetts, United States.

Thompson, C., Smith, L., & Maji, R. (2007). Hydrogeological modeling of submarine groundwater discharge on the continental shelf of Louisiana. *Journal of Geophysical Research*, *112*, C03014. https://doi.org/10.1029/2006JC003557

Toole, J. M., Andres, M., Le Bras, I. A., Joyce, T. M., & McCartney, M. S. (2017). Moored observations of the Deep Western Boundary Current in the NW Atlantic: 2004–2014. *Journal of Geophysical Research: Oceans*, *122*, 7488–7505. https://doi.org/10.1002/2017JC012984

Tryon, M., Brown, K., Dorman, L., & Sauter, A. (2001). A new benthic aqueous flux meter for very low to moderate discharge rates. *Deep Sea Research Part I: Oceanographic Research Papers*, *48*(9), 2121–2146. https://doi.org/10.1016/S0967-0637(01)00002-4

Werner, A. D., Bakker, M., Post, V. E. A., Vandenbohede, A., Lu, C., Ataie-Ashtiani, B., et al. (2013). Seawater intrusion processes, investigation and management: Recent advances and future challenges. *Advances in Water Resources*, *51*(Supplement C), 3–26. https://doi.org/10.1016/j.advwatres.2012.03.004

Wheat, C. G., Mottl, M. J., Fisher, A. T., Kadko, D., Davis, E. E., & Baker, E. (2004). Heat flow through a basaltic outcrop on a sedimented young ridge flank. *Geochemistry, Geophysics, Geosystems*, *5*, Q12006. https://doi.org/10.1029/2004GC000700

Wilson, A., & Ruppel, C. (2007). Salt tectonics and shallow subseafloor fluid convection: Models of coupled fluid-heat-salt transport. *Geofluids*, *7*(4), 377–386. https://doi.org/10.1111/j.1468-8123.2007.00191.x

Wilson, A. M. (2003). The occurrence and chemical implications of geothermal convection of seawater in continental shelves. *Geophysical Research Letters*, *30*(21), 2127. https://doi.org/10.1029/2003GL018499

Wilson, A. M. (2005). Fresh and saline groundwater discharge to the ocean: A regional perspective. *Water Resources Research*, *41*, W02016. https://doi.org/10.1029/2004WR003399

Wilson, A. M., Evans, T., Moore, W., Schutte, C. A., Joye, S. B., Hughes, A. H., & Anderson, J. L. (2015). Groundwater controls ecological zonation of salt marsh macrophytes. *Ecology*, *96*(3), 840–849. https://doi.org/10.1890/13-2183.1

Wilson, A. M., Woodward, G. L., & Savidge, W. B. (2016). Using heat as a tracer to estimate the depth of rapid porewater advection below the sediment–water interface. *Journal of Hydrology*, *538*, 743–753. https://doi.org/10.1016/j.jhydrol.2016.04.047

Wright, J. A., & Louden, K. E. (1989). *CRC handbook of seafloor heat flow*. Boca Raton, Florida: CRC Press, Inc.

Zektser, I. S., & Dzhamalov, R. G. (2007). In L. G. Everett (Ed.), *Submarine groundwater*. Boca Raton, Florida: CRC Press, Inc.